Biophysical Journal Volume 104 March 2013 1029–1037

Fusion Peptides Promote Formation of Bilayer Cubic Phases in Lipid Dispersions. An X-Ray Diffraction Study

Boris G. Tenchov,[†‡*] Robert C. MacDonald,[‡] and Barry R. Lentz[§]

[†]Department of Medical Physics and Biophysics, Medical University Sofia, Sofia, Bulgaria; [‡]Biochemistry, Molecular Biology and Cell Biology Department, Northwestern University, Evanston, Illinois; and [§]Department of Biochemistry & Biophysics and Program in Molecular & Cellular Biophysics, University of North Carolina, Chapel Hill, North Carolina

ABSTRACT Small angle x-ray diffraction revealed a strong influence of the N-terminal influenza hemagglutinin fusion peptide on the formation of nonlamellar lipid phases. Comparative measurements were made on a series of three peptides, a 20-residue wild-type X-31 influenza virus fusion peptide, GLFGAIAGFIENGWEGMIDG, and its two point-mutant, fusion-incompetent peptides G1E and G13L, in mixtures with hydrated phospholipids, either dipalmitoleoylphosphatidylethanolamine (DPoPE), or monomethylated dioleoyl phosphatidylethanolamine (DOPE-Me), at lipid/peptide molar ratios of 200:1 and 50:1. All three peptides suppressed the H_{II} phase and shifted the L_{α}–H_{II} transition to higher temperatures, simultaneously promoting formation of inverted bicontinuous cubic phases, Q_{II}, which becomes inserted between the L_{α} and H_{II} phases on the temperature scale. Peptide-induced Q_{II} had strongly reduced lattice constants in comparison to the Q_{II} phases that form in pure lipids. Q_{II} formation was favored at the expense of both L_{α} and H_{II} phases. The wild-type fusion peptide, WT-20, was distinguished from G1E and G13L by the markedly greater magnitude of its effect. WT-20 disordered the L_{α} phase and completely abolished the H_{II} phase in DOPE-Me/WT-20 50:1 dispersions, converted the Q_{II} phase type from Im3m to Pn3m and reduced the unit cell size from ~38 nm for the Im3m phase of DOPE-Me dispersions to ~15 nm for the Pn3m phase in DOPE-Me/WT-20 peptide mixtures. The strong reduction of the cubic phase lattice parameter suggests that the fusion-promoting WT-20 peptide may function by favoring bilayer states of more negative Gaussian curvature and promoting fusion along pathways involving Pn3m phase-like fusion pore intermediates rather than pathways involving H_{II} phase-like intermediates.

INTRODUCTION

Viral fusion proteins are known to contain segments of 10–30 mostly nonpolar residues, so-called fusion peptides (FPs), which insert into the host cell membrane at an early stage of fusion. According to the consensus picture, their insertion is associated with a sequence of events, involving viral protein conformational transitions, which finally result in merging of the viral membrane into the target membrane (1). Although this picture suggests that FPs serve to attach the viral protein to the host membrane, this does not appear to be their only function. In vitro studies have typically proposed that FPs alone, at sufficiently high peptide/lipid ratios display an ability to promote membrane rupture or fusion (2–8). More specifically, the wild-type fusion peptide (WT-20) from X-31 influenza virus hemagglutinin fusion protein (HA) does not induce fusion in phosphatidylcholine vesicles but does promote polyethylene glycol (PEG)-mediated fusion (9). At high peptide/lipid ratios (> ~1/200) in the absence of PEG, the peptide promoted aggregation, rupture, and formation of a precipitate. Despite advances in determination of the membrane localization and conformation of FPs (10), the mechanisms by which such peptides render the bilayers more fusogenic are unclear. It is often said that the HA FP destabilizes or perturbs the lipid bilayers—somewhat vague notions that provide little structural insight.

Insertion of peptides into a membrane may affect its curvature. Indeed, studies with a number of small FPs have shown that these peptides have an impact on the lamellar-inverted hexagonal (Lα–HII) transition temperature and may induce formation of isotropic phases (detected by NMR) or cubic phases (detected by x-ray diffraction (XRD)) (11–19). A possible interpretation of these results is that membranes could acquire negative curvature in the presence of FPs, and that FPs may thus facilitate formation of curved stalks that develop into fusion pores. Unsolved problems and ambiguities nevertheless still prevail. A quantitative description of how FPs affect the stabilities of the different inverted phases, both among themselves and relative to the lamellar phase, is still lacking and this circumstance by itself is sufficient to preclude further insights into the mode of action of these peptides.

There is evidence that conversion of lamellar to inverted bicontinuous cubic phase proceeds via intermediates that are expected to be isomorphous to fusion pores (Fig. 1 (20)). Based on this similarity, we consider the transformation from lamellar into inverted bicontinuous cubic phase as a generic model of fusion pore formation. Although a lamellar phase consists of multiple, separate bilayers, the bicontinuous cubic phase consists of a single bilayer draped along an infinite periodic minimal surface (IPMS). It is thus obvious that a lamellar-to-bilayer cubic phase transition actually involves multiple membrane fusion events.

Submitted August 17, 2012, and accepted for publication December 17, 2012.

*Correspondence: btenchov@gmail.com

Editor: Huey Huang.

0006-3495/13/03/1029/9 $2.00

http://dx.doi.org/10.1016/j.bpj.2012.12.034

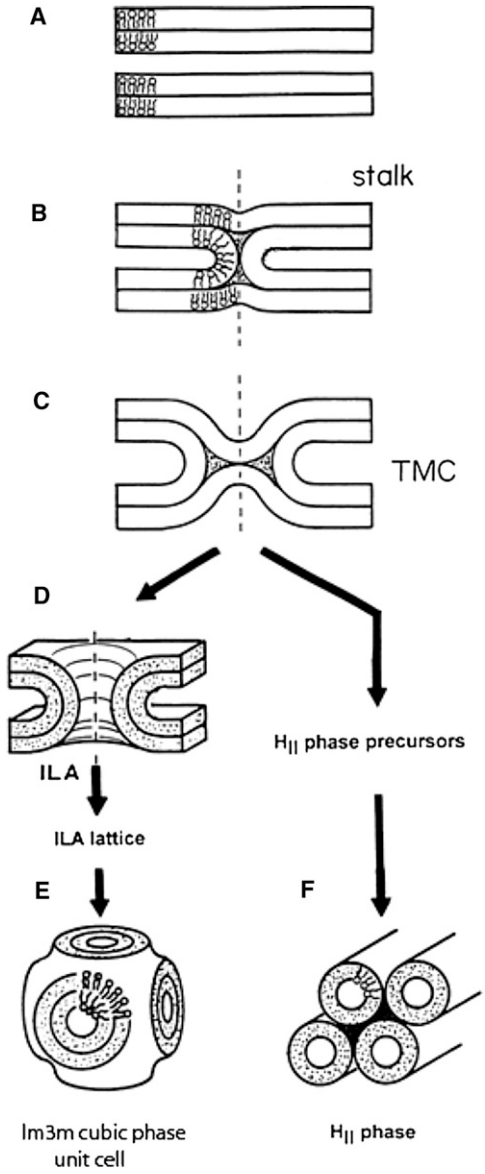

FIGURE 1 The modified stalk mechanism of membrane fusion and inverted phase formation. (*A*) Planar lamellar (L_α) phase bilayers; (*B*) the stalk intermediate; the stalk is cylindrically symmetrical about the dashed vertical axis; (*C*) the TMC (trans monolayer contact) or hemifusion structure; the TMC can rupture to form a fusion pore, referred to as interlamellar attachment, ILA (*D*); (*E*) If ILAs accumulate in large numbers, they can rearrange to form Q_{II} phases. (*F*) For systems close to the L_α/H_{II} phase boundary, TMCs can also aggregate to form H_{II} precursors and assemble into H_{II} domains (reproduced from (20) with permission).

Following this reasoning, it becomes of interest to clarify the effect of fusion peptides on lipid transformations from lamellar into nonlamellar phases such as hexagonal and/or bicontinuous cubic phases. In this investigation we applied time-resolved XRD to characterize the effects of a series of three peptides, the wild-type N-terminal influenza hemagglutinin fusion peptide (WT-20) and two of its mutants, G1E and G13L, on the phase behavior of phospholipids known to display lamellar-to-nonlamellar phase transformations. We show here that all three peptides promote formation of inverted cubic phase at the expense of the adjacent lamellar and inverted hexagonal phases, but that the effect of the wild-type peptide is much stronger than that of the two mutants.

MATERIALS AND METHODS

Three 20-residue peptides were used, the wild-type N-terminal influenza X-31 hemagglutinin fusion peptide, GLFGAIAGFIENGWEGMIDG and the mutant peptides G1E and G13L, with sequences **E**LFGAIAGFIENG WEGMIDG and GLFGAIAGFIEN**L**WEGMIDG, respectively. The peptides, with a purity of >90%, were synthesized at the peptide facility of the University of North Carolina, Chapel Hill, as described elsewhere (9). The phospholipids dipalmitoleoylphosphatidylethanolamine (DPoPE) and monomethylated dioleoyl phosphatidylethanolamine (DOPE-Me) were purchased from Avanti Polar Lipids and used as received. Both lipids were pure as judged by thin layer chromatography and displayed phase transitions in accord with published data. Lipid/peptide mixtures were prepared by mixing lipid solutions in chloroform with peptide solutions in dimethyl sulfoxide (DMSO). The solvents were removed by drying with argon, followed by extensive high-vacuum evacuation for 72 h, as necessary for complete removal of DMSO. The dry lipid/peptide films were hydrated in phosphate buffered saline (PBS), pH 7.2, or citrate buffer, pH 5, and homogenized by a succession of five freeze-thaw cycles between dry ice and room temperature, accompanied by vortexing during thawing. The lipid concentration in the dispersion was 10% (w/v). After their preparation, the lipid/peptide dispersions were stored at 4°C overnight and equilibrated at room temperature for several hours before the x-ray measurements. The samples were vortexed and loaded into x-ray capillaries immediately before their measurement.

X-ray measurements

Low-angle XRD patterns were recorded at stations 5IDD, DND-CAT, and 18D, BioCAT, APS, Argonne National Laboratory, using two-dimensional 2048 × 2048 MAR detectors at a sample-to-detector distance of ~200 cm. Spacings were determined from axially integrated two-dimensional images using the Fit2D program (21) and silver behenate as a calibration standard (*d*-spacing 5.838 nm (22)). Raw data are presented and no smoothing and background subtraction procedures have been applied. A temperature-controlled capillary sample holder was used. All measurements were started at 20°C. The exposure times for collection of the XRD patterns were in the range of 0.7–1 s. About 20–40 consecutive patterns were recorded to monitor the phase conversions. In this way, the irradiation times during the heating scan were limited to a total of 30–40 s. These times were several times shorter than the exposures of a few minutes needed to cause observable radiation damage in lipid dispersions under our experimental conditions.

Temperature protocols were executed directly on samples mounted on the beam line, and it was thus possible to follow in real time the phase conversions taking place in the lipid peptide dispersions. The sample holder was mounted on a remotely controlled motorized stage and, by moving the stage with respect to the incident x-ray beam, x-ray patterns could be recorded from different parts of the same sample. Such measurements—routinely made before and after the temperature scans—showed that the patterns recorded were representative of the entire sample volumes and that there were no systematic differences between irradiated and nonirradiated portions of the sample. Comparisons with dark samples subjected to the same temperature protocols, for which only the initial and final states were recorded, also confirmed the lack of radiation damage effects. On the basis of these tests, we consider the results reported here as not influenced by radiation damage of the lipid.

RESULTS

In addition to the lamellar liquid crystalline L_α and inverted hexagonal H_{II} phases, fully hydrated DPoPE and DOPE-Me dispersions can also form inverted bicontinuous cubic Q_{II} phases under appropriate temperature protocols. We use these systems in this work to characterize the effects of HA FP and its two mutants on the relative stability of the lamellar and nonlamellar lipid phases. To expose more clearly the FP effects, we used 10 wt % lipid dispersions in which the cubic phase formation is strongly facilitated relative to that in the more concentrated dispersions typically used in x-ray studies.

Phase behavior of DPoPE/FP mixtures

In the absence of peptides, DPoPE dispersions display a cooperative, sharp lamellar liquid crystalline-inverted hexagonal ($L_\alpha \rightarrow H_{II}$) phase transition at ~42°C (23). As is generally typical for the phosphatidylethanolamines (PEs), this transition is not fully reversible and the recovery of the initial L_α phase in the backward transition is accompanied by the formation of a trace amount of cubic Pn3m phase (Fig. 2 *A*). The x-ray data presented here show that the FPs strongly influences the lamellar-nonlamellar transformations in DPoPE. In particular, they suppress the H_{II} phase and promote cubic phase formation. The effects of the wild-type peptide (WT-20) were much more pronounced than those of the mutant peptides G1E and G13L (Figs. 2 and 3). At a lipid/peptide ratio of 50:1, WT-20 almost fully suppressed the recovery of the L_α phase in the cooling transition (Figs. 2 *B* and 3). In contrast to the behavior of the pure lipid, in which traces of cubic phase appear during the cooling transition only, the DPoPE/WT-20 mixtures formed a cubic phase even on heating, concurrently with the $L_\alpha \rightarrow H_{II}$ phase transition (Fig. 2 *B*). The evolution of the Pn3m lattice constants in a heating-cooling cycle (Fig. 4) was typical for PE cubic phases (24). The lattice constants decrease on heating and increase on cooling in the temperature range of the H_{II} phase, and level off in the temperature range of the L_α phase. At the end of the temperature cycle, the values of the Pn3m lattice constants for the different peptides were in the following order: control (no peptide) > G1E > G13L > WT-20 (Fig. 4, Table 1), indicating that the peptides promoted formation of highly curved bicontinuous cubic structures. Promotion of the cubic phase by the FPs involved suppression of the H_{II} phase. The FPs noticeably broadened and shifted to higher

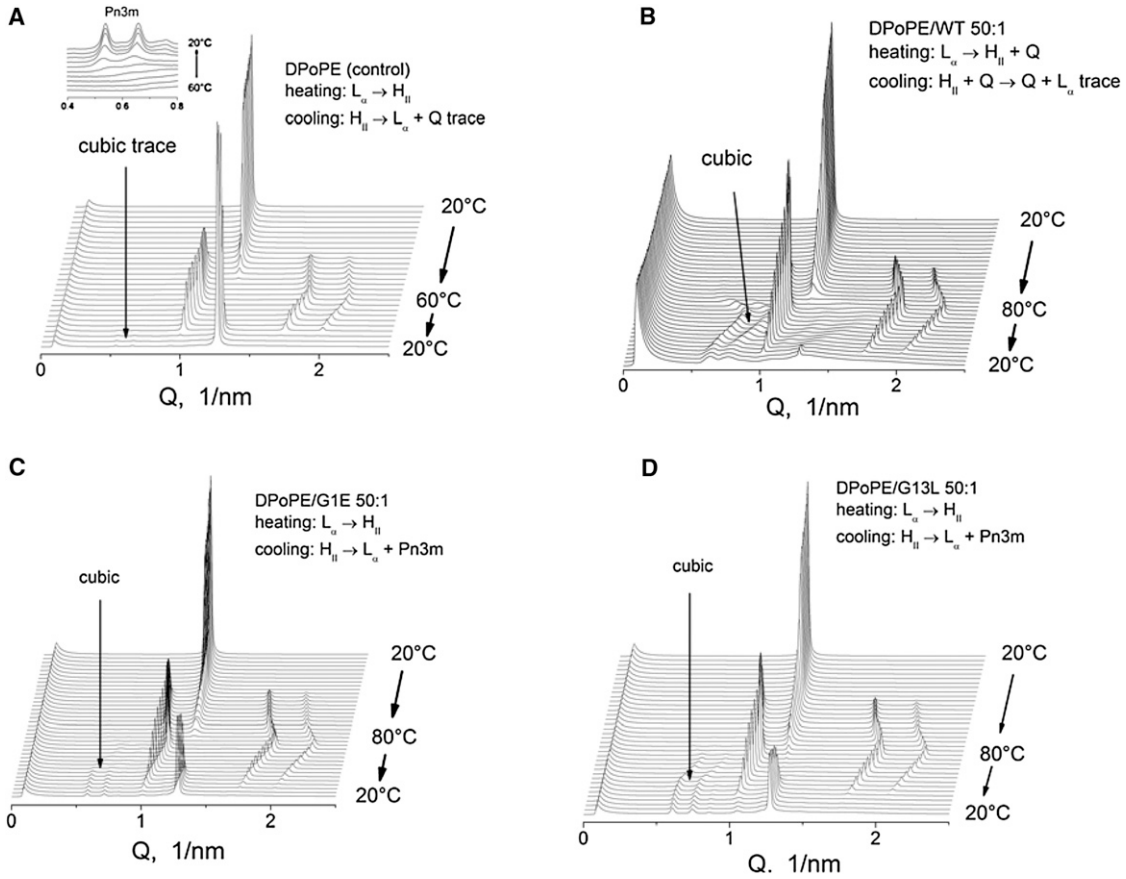

FIGURE 2 Sequences of XRD patterns recorded during heating-cooling scans of DPoPE/fusion peptide mixtures (heating 1°C/min, cooling 3°C/min). (*A*) DPoPE control (no peptide); (*B*) DPoPE/WT-20; (*C*) DPoPE/G1E; (*D*) DPoPE/G13L. Lipid/peptide molar ratios 50:1.

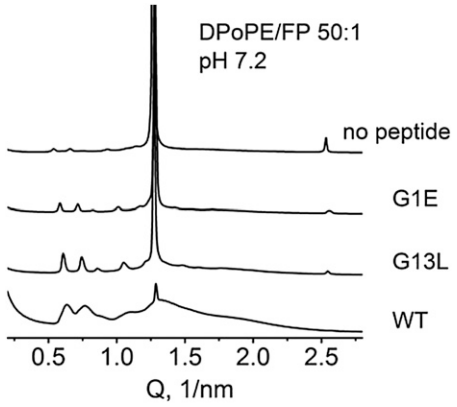

FIGURE 3 Comparison of the XRD patterns recorded at 20°C from DPoPE/fusion peptide mixtures after heating-cooling scans shown in Fig. 2. The lattice parameters of the phases are summarized in Table 1.

temperatures the $L_\alpha \rightarrow H_{II}$ phase transition of DPoPE (Fig. 5). This effect was accompanied by a slight reduction of the L_α and H_{II} spacing (Fig. 6).

In summary, the FPs promoted Pn3m phase formation and suppressed the H_{II} phase of DPoPE. The effects of the WT-20 peptide were much stronger than those of the mutant peptides G1E and G13L. The magnitudes of their effects fall in the order WT-20 > G13L > G1E.

Phase behavior of DOPE-Me/FP mixtures

Due to their ability to easily form inverted cubic phases, DOPE-Me dispersions also represent an appropriate experimental system for evaluation of the FP effects on the lamellar-to-nonlamellar phase conversions. DOPE-Me dispersions are known to slowly transform from the lamellar phase into a thermodynamically stable Q_{II} phase during incubation at constant temperature in the range ~55–60°C. Concentrated dispersions (~30 wt %) form the Pn3m phase (25–27), whereas diluted dispersions (~10–15 wt %) form the Im3m cubic phase (28,29), in accord with the behavior of other PEs (24) (the unit cell of the Im3m phase is shown in Fig. 1). The lamellar to Im3m phase transformation can

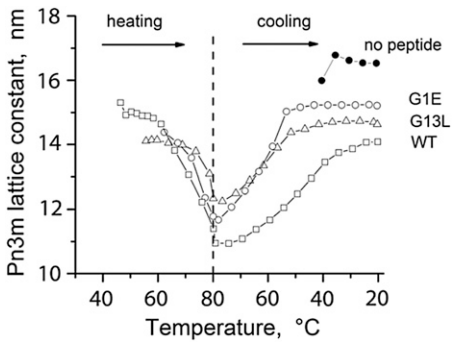

FIGURE 4 Evolution of the Pn3m phase lattice parameter of DPoPE/fusion peptide dispersions during heating-cooling cycles.

TABLE 1 Lattice parameters of DPoPE and DOPE-Me mixtures with fusion peptides at 20°C

Lipid	Lipid/peptide ratio		Phase[a]	No peptide	G1E	G13L	WT-20
DPoPE	50:1	Initial	L_α	4.96	4.88	4.89	4.92
(pH 7.2)		Final	L_α	4.96	4.91	4.94	4.88
		Final	Pn3m	16.5	15.2	14.6	14.0
DOPE-Me		Initial	L_α	6.26/6.40[b]			
(pH 7.2)	50:1	Final	Im3m	37.5	[34.2]	37.3	[18.9]
		Final	Pn3m	[29.3]	26.7	28.8	14.8
DOPE-Me	50:1		Im3m	38.2	34.4	30.3	20.5
(pH 5.0)			Pn3m	[29.8]	26.8	24.3	16.1
DOPE-Me	200:1		Im3m	37.5	34.7	36.1	24.2
(pH 7.2)			Pn3m	[29.3]	27.3	28.2	19.0

Initial and final denote values obtained before and after a heating-cooling cycle, respectively. Lattice constants in the square brackets were calculated using the Im3m/Pn3m lattice constant ratio of 1.28, which follows from the Bonnet transformation between these phases (see the text for details).
[a]The lattice constants of the Im3m and Pn3m vary in a range of ±2 nm in different measurements.
[b]L_α spacing of DOPE-Me dispersions at 50°C.

also be induced in diluted DOPE-Me dispersions in a single heating-cooling cycle ($L_\alpha \rightarrow H_{II}$ in the heating direction, followed by $H_{II} \rightarrow$ Im3m in the cooling direction) carried out at relatively fast scan rates (Fig. 7 *A*). Examples of these two routes for induction of Q_{II} phases (slow conversion at constant temperature versus heating followed by cooling) in diluted DOPE-Me dispersions are given in our previous work (28,29). Both methods resulted in formation of Im3m cubic phases at ~55°C with identical x-ray patterns and similar lattice spacings, typically in the range 35–40 nm. On this basis, it was concluded that, like the constant temperature incubation, the cooling $H_{II} \rightarrow$ Im3m transition in a heating-cooling cycle also results in formation of an equilibrium Im3m cubic phase in 10 wt % DOPE-Me dispersions, even though the cooling scans were performed at relatively high scan rates of 1–5°C/min (29). Once formed at ~55°C, either by $L_\alpha \rightarrow$ Im3m transition during constant temperature incubation or by $H_{II} \rightarrow$ Im3m transition in

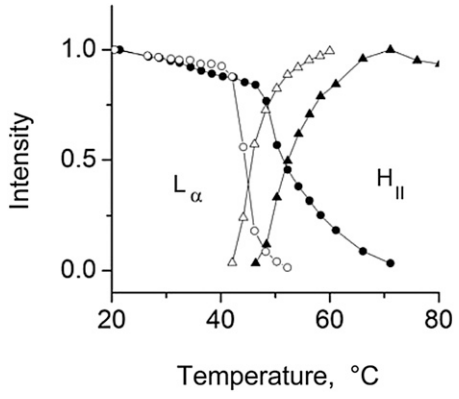

FIGURE 5 Upward shift of the $L_\alpha \rightarrow H_{II}$ transition in a 50:1 DPoPE/WT-20 50:1 mixture (*solid symbols*) with respect to the pure DPoPE dispersions (*open symbols*).

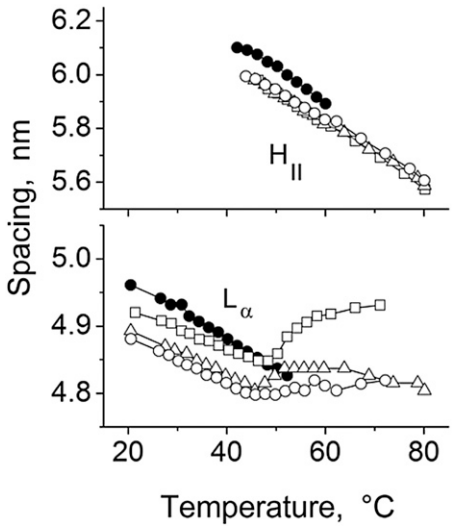

FIGURE 6 L_α and H_{II} spacings of DPoPE (*solid symbols*) and 50:1 DPoPE/fusion peptide mixtures: WT-20 (*squares*), G1E (*triangles*), G13L (*circles*).

a cooling scan, the Im3m phase does not change upon cooling to 20°C and exists for an indefinitely long time at room temperature (although it might actually be metastable with respect to the L_α phase at the latter temperatures). DOPE-Me thus provides a phospholipid system that appears to achieve an equilibrium cubic phase on an experimentally convenient timescale. Because the temperature cycle protocol is more time efficient, we chose it for characterization of the FP effects on DOPE-Me phases.

Similar to their effects on DPoPE dispersions, FPs also suppressed the formation of the H_{II} phase and facilitated cubic phase formation in DOPE-Me dispersions. The behavior of WT-20/DOPE-Me mixtures is shown in Fig. 8, *B* and *C*. Upon heating at a peptide/lipid molar ratio of 1:200, the L_α phase disappeared at 60°C, the onset of the H_{II} phase was shifted from ~62 to ~72°C, and an intermediate cubic phase with gradually decreasing lattice constant formed in the range 60–72°C. The H_{II} phase disappeared at 61°C on cooling and was replaced by a mixture of Im3m and Pn3m phases with lattice spacings of 24.2 and 19.0 nm, respectively, after cooling to 20°C (Table 1). A higher peptide concentration of 1:50 peptide/lipid ratio resulted in disordering of the DOPE-Me L_α phase. However, after heating and cooling the disordered phase became converted into a well-organized Pn3m phase with a relatively short spacing of 14.8 nm (Fig. 7 *C*; Table 1). No H_{II} phase was found to form in 1:50 peptide/lipid samples at temperatures up to 80°C. Again, the mutant peptides G1E and G13L displayed weaker effects on DOPE-Me L_α and H_{II} phases. They did not dissipate the L_α phase, suppressed the H_{II} phase to a much smaller extent than did WT-20 (Fig. 8), and produced significantly smaller reductions of the cubic phase lattice constants (Fig. 9, Table 1). Summing up, the addition of FPs resulted in shortening of the cubic phase lattice parameter and transformation of the initial Im3m phase of pure

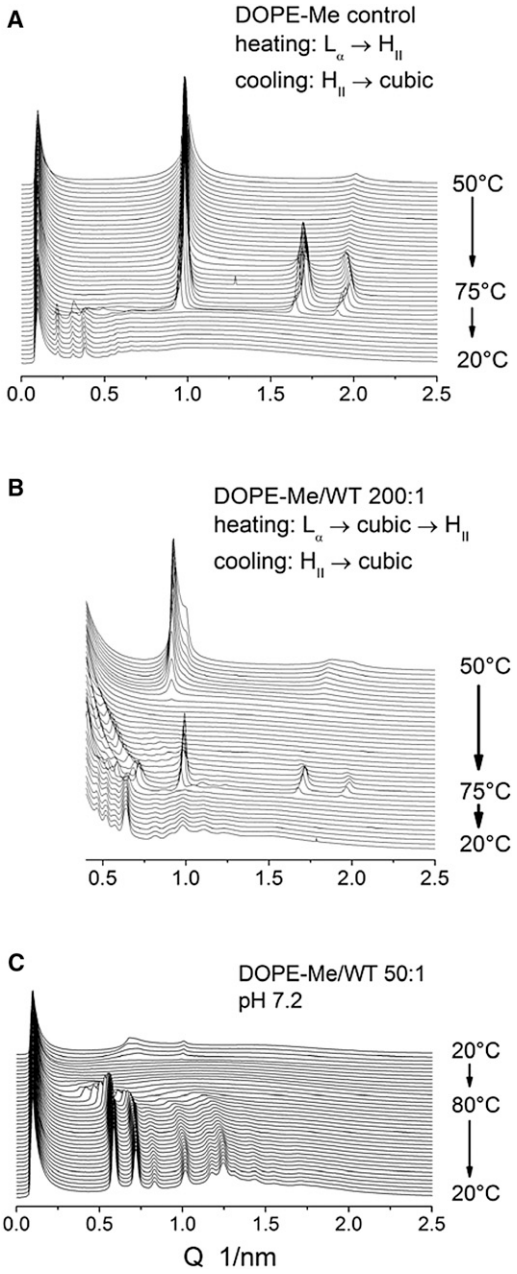

FIGURE 7 Phase conversions during heating (1°C/min) and cooling (5°C/min) of 10 wt % DOPE-Me dispersions (*A*) and DOPE-Me/WT-20 mixtures at molar ratios 200:1 (*B*) and 50:1 (*A*). PBS, pH 7.2. The cubic phase lattice constants are (*A*) Im3m 38 nm; (*B*) Im3m 24.2 nm/Pn3m 19.0 nm mixture; (*C*) Pn3m 14.8 nm (Table 1).

DOPE-Me with an Im3m/Pn3m mixture or a single Pn3m phase. Because the lattice parameters of the Im3m and Pn3m phases cannot be directly compared, to quantitate the lattice shrinking caused by the FPs, we note that the Im3m/Pn3m lattice parameter ratios in all cases of coexisting Im3m and Pn3m pairs were equal with good accuracy to 1.28, in agreement with earlier observations on coexisting cubic phases in diluted phospholipid dispersions (24), and in compliance with the value obtained on the basis of the

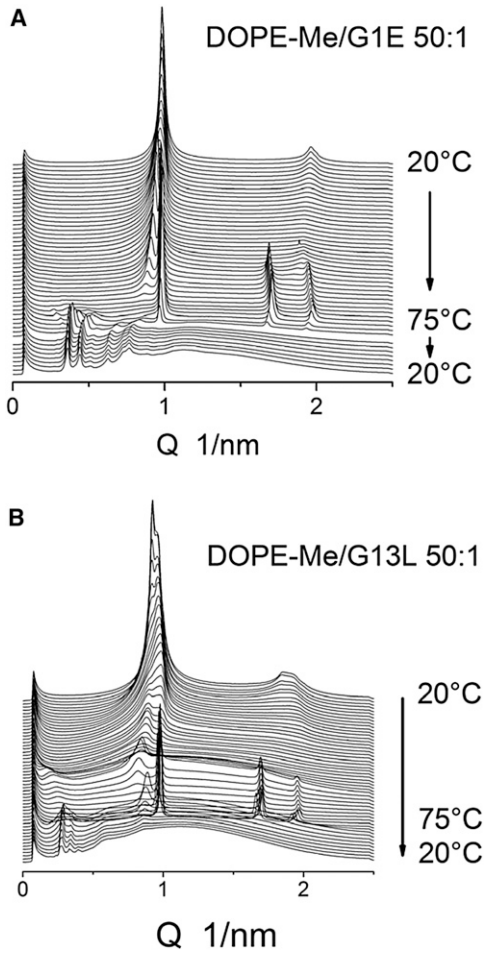

FIGURE 8 Phase transformations during heating (1°C/min) and cooling (5°C/min) of 10 wt % DOPE-Me/G1E (*A*) and DOPE-Me/G13L (*B*) mixtures at lipid/peptide molar ratio 50:1. The lattice constants of the final cubic phases are given in Table 1.

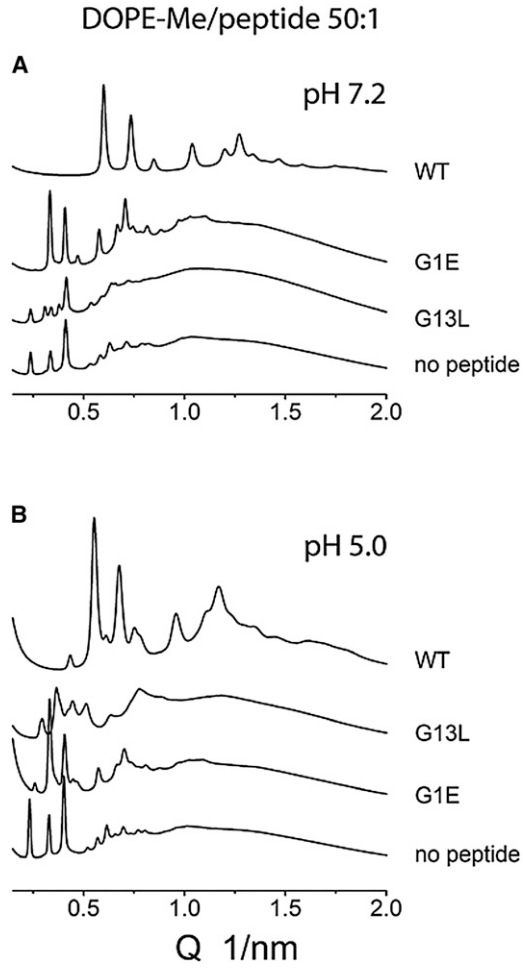

FIGURE 9 Comparison of XRD patterns recorded at 20°C from DOPE-Me/fusion peptide (50:1) mixtures after heating-cooling scans. (*A*) pH 7.2; (*B*) pH 5.0. The lattice constants of the cubic phases are summarized in Table 1.

Im3m and Pn3m representation with the primitive (P) and diamond (D) IPMS, respectively. Considerations based on the Bonnet transformation between these IPMS, which involves the gyroid IPMS as an intermediate (30), or, alternatively, based on a direct Im3m-Pn3m transformation pathway proposed in (31), showed that the ratio of the unit cell dimensions of the Im3m and Pn3m phases, linked by these transformations, must be equal to 1.28. We can thus use this ratio to calculate the lattice parameter of the conjugated cubic phase in the cases where we observed a single Im3m or Pn3m phase. The values calculated in this way are given in square brackets in Table 1. These values complement the experimentally measured lattice parameters and provide a quantitative measure of the reduction of the cubic phase lattice parameters induced by the FPs.

DISCUSSION

The fusion peptides all promoted formation of the Q_{II} phase at the expense of both the L_α and H_{II} phases. They suppressed and shifted to higher temperatures the H_{II} phases of DPoPE and DOPE-Me, most dramatically in the case of the WT-20 peptide, which completely abolished the H_{II} phase and disordered the L_α phase in DOPE-Me/WT-20 50:1 dispersions (Fig. 7 *C*). All three peptides reduced the unit cell sizes of the cubic phases, but the effect of WT-20 was particularly strong. At a DOPE-Me/peptide 50:1 molar ratio, the presence of WT-20 resulted in formation of a Q_{II} phase with ~2 times smaller lattice constant than was found in the presence of the mutant peptides (Table 1). WT-20 converted the cubic phase type from Im3m to Pn3m and reduced the unit cell size from ~38 nm for the Im3m phase in DOPE-Me dispersions to ~15 nm for the Pn3m phase in DOPE-Me/peptide mixtures. The formation of inverted bicontinuous cubic structures of smaller lattice constants in the presence of fusion peptides implies that fusion peptides promote more negative Gaussian curvature of the lipid bilayers because the surface-averaged Gaussian curvature in the cubic unit cell

is proportional to $-1/a^2$, where a is the lattice parameter of the cubic phase (32).

The markedly different effects of WT-20 and the mutant peptides G1E and G13L on the lipid phase behavior appear to be consistent with differences in their molecular structures. The N-terminal segments of the influenza virus glycoprotein HA2 domains modeled by the synthetic fusion peptides are represented by hydrophobic, highly conserved glycine-rich sequences. Comparisons of these sequences in various subtypes of influenza virus strains have demonstrated that the residues Gly-1–Glu-11, Gly-13, Trp-14, and Gly-16 are strictly conserved (8,33–35). The Gly-1 N-terminal residue is particularly critical for the fusion function. Substitution of glutamic acid for Gly-1 completely abolishes HA protein fusion activity (36) and substitutions with other amino acids, Ala, Ser, Val, Glu, Gln, or Lys, result in substantial impairments of the fusion phenotype (37). NMR and spin labeling studies of the WT-20 peptide coupled at its C-terminus to NH2-GCGKKKK-CONH2 showed that it adopts an inverted V-shaped conformation in micelles and lipid bilayers with a kink angle of 105° formed by Glu-11, Asn-12, and Gly-13 (38,39). The C-terminal segment of the peptide forms an amphipathic helix at the membrane interface, whereas the N-terminal segment is deeply embedded in the hydrophobic interior of the bilayer. Due to the highly hydrophilic nature of Glu, one may expect that replacing Gly-1 with Glu would result in reduced hydrophobic penetration of the N-terminus of G1E. Another strictly conserved glycine residue, Gly-13, is part of the short structural motif forming the kink and stabilizing the peptide V-shaped conformation in the membrane. A study on a set of fusion peptide sequences suggests that substituting Gly-13 by leucine may destabilize and eliminate the kink modifying in this way the conformation of G13L in the bilayers (8). Another G13 mutation, G13A, was found to result in a shallower kink conformation with a kink angle increased from 105°C in the wild-type peptide to 150°C in the G13A mutant (40). It thus appears that the unique WT-20 conformation in the membrane is particularly important for the profound WT-20 effects on the PE phase behavior (destabilization of the L_α and H_{II} phases in favor of Q_{II} formation and strongly reduced Q_{II} lattice spacing), because these effects are displayed to a much lesser extent in PE mixtures with the mutant G1E and G13L peptides. Notably, the smaller effects of the mutant peptides relative to WT-20 correlate with their reduced fusion-promoting ability in PEG-mediated model membrane fusion and reduced influence on the hydrophobic interior of the bilayer assessed on the basis of circular dichroism, Fourier transform infrared spectroscopy, and fluorescence probe data (41). Despite the significant progress in the elucidation of the WT-20 conformation in lipid bilayers, it remains unclear at molecular level how the FPs stabilize more negative Gaussian curvatures and bring about a substantial reduction of the Im3m and Pn3m lattice parameters. Because the respective IPMS consist of saddle points with equal in magnitude and opposite in sign principal curvatures (resulting in zero mean curvature), one may speculate that the FPs create local directionality at the membrane surface such that the lipid monolayer bends in opposite directions along the peptide contour and in a perpendicular to it direction. Considerations of the molecular interactions of basic arginine residues with the lipid surface groups have led to the conclusion that cell-penetrating arginine-rich peptides can generate positive curvature along their length and negative curvature in perpendicular direction, thus promoting negative Gaussian curvature and formation of a Pn3m cubic phase (42). Although these considerations do not appear to be directly applicable to the FPs studied in this work, it is thinkable, for example, that the rigid V-shaped conformation of WT-20 might be instrumental in promoting a positive monolayer curvature along the peptide contour, in combination with negative curvature (membrane wrapping around the peptide) in perpendicular direction. Such a picture would be consistent with the observed smaller effects of the mutant FPs, which likely result from a destabilized V-shape as discussed previously, and with the gradual decrease of the cubic phase lattice parameter with increase of the FP concentration. However, it is appropriate to note that, besides the fusion peptides, a number of other peptides, e.g., pore-forming antimicrobial peptides were also found to promote cubic phase formation (43–47). It would be of significant interest to compare the structures of the different peptides known to induce cubic phases with the hope of distinguishing whether these peptides generate negative Gaussian curvatures by a unique or by different molecular mechanisms.

At temperatures below the onset of H_{II} and Q_{II} phase formation, we observed L_α phase disordering (loss of correlation between adjacent bilayers and L_α unbinding) in DOPE-Me mixtures with WT-20, but not with the G1E and G13L mutants. The WT-20 peptide induced almost complete disordering of the L_α phase in DOPE-Me, followed by facile conversion into the inverted cubic phase (Fig. 7 *C*), whereas the mutant peptides G1E and G13L had much smaller effects (Fig. 8). In a previous study, we showed that unbinding of the L_α phase is an important factor in facilitating inverted cubic phase formation (28). An L_α phase disordering was also found in mixtures of supported dioleoyl phosphatidylcholine (DOPC) multilayers with HIV-1 fusion peptide (48,49). It was argued that the disordering of the DOPC L_α phase could be due either to electrostatic repulsion between the bilayers resulting from uncompensated surface charge introduced by the peptide molecules, or to a repulsive force arising from increased out-of-plane membrane undulations, seen as deriving from a decreased membrane bending modulus. The present comparative study of three different peptides provides some clues about the origin of the unbinding effect. Taking note of the much stronger disordering effect of WT-20 versus

the mutant peptides on the L_α phase, it appears unlikely that the L_α phase disordering of DOPE-Me is due to electrostatic repulsion. An electrostatic repulsive term should be the same for WT-20 and G13L, which have identical ionization states, or even stronger for G1E than for WT-20 due to an additional ionized group in the G1E mutant. It is similarly unlikely that unbinding could result from steric hindrance created by peptide chains occupying space at the membrane interface. If present, a steric repulsion term could be expected to be of the same magnitude or even greater for the mutant peptides and would thus not explain why only WT-20 disorders the lamellar phase. On the other hand, WT-20 might have a stronger effect on the membrane mechanical properties than G1E and G13L due to its presumably deeper hydrophobic penetration. Thus, we believe that repulsion arising from out-of-plane membrane fluctuations induced by WT-20 is a more probable cause of the L_α phase unbinding than electrostatic or steric repulsion. If so, the L_α phase disordering induced in DOPC by HIV-1 fusion peptide (48,49) and in DOPE-Me by WT-20 may have a similar origin in a peptide-induced decrease of the bending energy.

The L_α phase disordering may also involve formation of Q_{II} phase precursors (fusion pores) at temperatures below the onset of the L_α-Q_{II} phase transformation. Lamellar phase disordering occurs also in pure DOPE-Me at temperatures in the range of the latter transition either during slow heating scans (26), or at constant temperature incubation (28,29). However, because WT-20 strongly favors Q_{II} at the expense of the lamellar phase, it must also facilitate formation of fusion pores at lower temperatures. Thus, one function of the fusion peptide in influenza HA-induced fusion may be to stabilize the fusion product by expanding to lower temperatures the temperature range in which fusion between bilayers can take place.

CONCLUSIONS

The present XRD study revealed a strong influence of N-terminal influenza hemagglutinin fusion peptides on the formation of inverted nonlamellar phospholipid phases. Measurements on phospholipid mixtures with the wild-type WT-20 peptide or its mutants G1E and G13L showed that the fusion peptides promote formation of cubic phases with substantially reduced lattice constant, which become inserted between the L_α and H_{II} phases. The cubic phase formation is favored at the expense of both L_α and H_{II} phases.

The effects of WT-20 are notably stronger than those of the G1E and G13L peptides. At a lipid/peptide molar ratio of 50:1, the WT-20 peptide completely abolishes the H_{II} phase and brings about almost complete unbinding of the L_α phase in DOPE-Me dispersions, followed by its facile replacement with a Pn3m cubic phase. The data suggest that the fusion-competent WT-20 peptide may act specifically by favoring membrane states of more negative Gaussian curvature and promoting fusion along pathways involving inverted cubic (Pn3m) phase-like structures rather than pathways involving inverted hexagonal phase-like structures. The stronger effects of WT-20 in comparison to the effects of the G1E and G13L mutant peptides appear to be due to its deeper penetration into the hydrophobic membrane core.

We thank Dr. David Siegel for useful discussions on the data interpretation. Synchrotron x-ray measurements were performed at DND-CAT and Bio-CAT at APS, Argonne National Laboratory. We thank the Argonne National Laboratory for the use of the Advanced Photon Source (APS), supported by the U. S. Department of Energy.

This work was supported by National Institutes of Health (NIH) GM 57305 and GM 32707.

REFERENCES

1. Lentz, B. R., V. Malinin, …, K. Evans. 2000. Protein machines and lipid assemblies: current views of cell membrane fusion. *Curr. Opin. Struct. Biol.* 10:607–615.
2. Nieva, J. L., S. Nir, and J. Wilschut. 1998. Destabilization and fusion of zwitterionic large unilamellar lipid vesicles induced by a beta-type structure of the HIV-1 fusion peptide. *J. Liposome Res.* 8:165–182.
3. Wharton, S. A., S. R. Martin, …, D. C. Wiley. 1988. Membrane fusion by peptide analogues of influenza virus haemagglutinin. *J. Gen. Virol.* 69:1847–1857.
4. Lear, J. D., and W. F. DeGrado. 1987. Membrane binding and conformational properties of peptides representing the NH2 terminus of influenza HA-2. *J. Biol. Chem.* 262:6500–6505.
5. Murata, M., Y. Sugahara, …, S. Ohnishi. 1987. pH-dependent membrane fusion activity of a synthetic twenty amino acid peptide with the same sequence as that of the hydrophobic segment of influenza virus hemagglutinin. *J. Biochem.* 102:957–962.
6. Rafalski, M., A. Ortiz, …, J. Wilschut. 1991. Membrane fusion activity of the influenza virus hemagglutinin: interaction of HA2 N-terminal peptides with phospholipid vesicles. *Biochemistry.* 30:10211–10220.
7. Bailey, A. L., M. A. Monck, and P. R. Cullis. 1997. pH-Induced destabilization of lipid bilayers by a lipopeptide derived from influenza hemagglutinin. *BBA-Biomembranes.* 1324:232–244.
8. Matsumoto, T. 1999. Membrane destabilizing activity of influenza virus hemagglutinin-based synthetic peptide: implications of critical glycine residue in fusion peptide. *Biophys. Chem.* 79:153–162.
9. Haque, M. E., A. J. McCoy, …, B. R. Lentz. 2001. Effects of hemagglutinin fusion peptide on poly(ethylene glycol)-mediated fusion of phosphatidylcholine vesicles. *Biochemistry.* 40:14243–14251.
10. Tamm, L. K., X. Han, …, A. L. Lai. 2002. Structure and function of membrane fusion peptides. *Biopolymers.* 66:249–260.
11. Yeagle, P. L., R. M. Epand, …, T. D. Flanagan. 1991. Effects of the 'fusion peptide' from measles virus on the structure of N-methyl dioleoylphosphatidylethanolamine membranes and their fusion with Sendai virus. *Biochim. Biophys. Acta.* 1065:49–53.
12. Epand, R. M., and R. F. Epand. 1994. Relationship between the infectivity of influenza virus and the ability of its fusion peptide to perturb bilayers. *Biochem. Biophys. Res. Commun.* 202:1420–1425.
13. Epand, R. F., I. Martin, …, R. M. Epand. 1994. Membrane orientation of the SIV fusion peptide determines its effect on bilayer stability and ability to promote membrane fusion. *Biochem. Biophys. Res. Commun.* 205:1938–1943.
14. Davies, S. M. A., R. F. Epand, …, R. M. Epand. 1998. Modulation of lipid polymorphism by the feline leukemia virus fusion peptide: implications for the fusion mechanism. *Biochemistry.* 37:5720–5729.

15. Siegel, D. P., and R. M. Epand. 2000. Effect of influenza hemagglutinin fusion peptide on lamellar/inverted phase transitions in dipalmitoleoylphosphatidylethanolamine: implications for membrane fusion mechanisms. *BBA-Biomembranes.* 1468:87–98.

16. Colotto, A., I. Martin, …, R. M. Epand. 1996. Structural study of the interaction between the SIV fusion peptide and model membranes. *Biochemistry.* 35:980–989.

17. Colotto, A., and R. M. Epand. 1997. Structural study of the relationship between the rate of membrane fusion and the ability of the fusion peptide of influenza virus to perturb bilayers. *Biochemistry.* 36:7644–7651.

18. Darkes, M. J. M., S. M. A. Davies, and J. P. Bradshaw. 1999. X-ray diffraction study of feline leukemia virus fusion peptide and lipid polymorphism. *FEBS Lett.* 461:178–182.

19. Harroun, T. A., K. Balali-Mood, …, J. P. Bradshaw. 2003. The fusion peptide of simian immunodeficiency virus and the phase behaviour of N-methylated dioleoylphosphatidylethanolamine. *BBA-Biomembranes.* 1617:62–68.

20. Siegel, D. P. 1999. The modified stalk mechanism of lamellar/inverted phase transitions and its implications for membrane fusion. *Biophys. J.* 76:291–313.

21. Hammersley, A. P., S. O. Svensson, …, D. Hausermann. 1996. Two-dimensional detector software: from real detector to idealised image or two-theta scan. *High Press. Res.* 14:235–248.

22. Huang, T. C., H. Toraya, …, Y. Wu. 1993. X-ray-powder diffraction analysis of silver behenate, a possible low-angle diffraction standard. *J. Appl. Cryst.* 26:180–184.

23. Koynova, R., and M. Caffrey. 1994. Phases and phase transitions of the hydrated phosphatidylethanolamines. *Chem. Phys. Lipids.* 69:1–34.

24. Tenchov, B., R. Koynova, and G. Rapp. 1998. Accelerated formation of cubic phases in phosphatidylethanolamine dispersions. *Biophys. J.* 75:853–866.

25. Gruner, S. M., M. W. Tate, …, P. R. Cullis. 1988. X-ray diffraction study of the polymorphic behavior of N-methylated dioleoylphosphatidylethanolamine. *Biochemistry.* 27:2853–2866.

26. Siegel, D. P., and J. L. Banschbach. 1990. Lamellar/inverted cubic (L alpha/QII) phase transition in N-methylated dioleoylphosphatidylethanolamine. *Biochemistry.* 29:5975–5981.

27. Cherezov, V., D. P. Siegel, …, M. Caffrey. 2003. The kinetics of non-lamellar phase formation in DOPE-Me: relevance to biomembrane fusion. *J. Membr. Biol.* 195:165–182.

28. Siegel, D. P., and B. G. Tenchov. 2008. Influence of the lamellar phase unbinding energy on the relative stability of lamellar and inverted cubic phases. *Biophys. J.* 94:3987–3995.

29. Tenchov, B., and R. Koynova. 2012. Cubic phases in membrane lipids. *Eur. Biophys. J.* 41:841–850.

30. Hyde, S. T., S. Andersson, …, K. Larsson. 1984. A cubic structure consisting of a lipid bilayer forming an infinite periodic minimum surface of the gyroid type in the glycerolmonooleate-water system. *Z. Kristallogr.* 168:213–219.

31. Charvolin, J., and J. F. Sadoc. 1996. Ordered bicontinuous films of amphiphiles and biological membranes. *Philos. Trans. R. Soc. Lond. Ser. A Math. Phys. Eng. Sci.* 354:2173–2192.

32. Templer, R. H., B. J. Khoo, and J. M. Seddon. 1998. Gaussian curvature modulus of an amphiphilic monolayer. *Langmuir.* 14:7427–7434.

33. Cross, K. J., W. A. Langley, …, D. A. Steinhauer. 2009. Composition and functions of the influenza fusion peptide. *Protein Pept. Lett.* 16:766–778.

34. Lorieau, J. L., J. M. Louis, and A. Bax. 2010. The complete influenza hemagglutinin fusion domain adopts a tight helical hairpin arrangement at the lipid:water interface. *Proc. Natl. Acad. Sci. USA.* 107: 11341–11346.

35. Nobusawa, E., T. Aoyama, …, K. Nakajima. 1991. Comparison of complete amino acid sequences and receptor-binding properties among 13 serotypes of hemagglutinins of influenza A viruses. *Virology.* 182: 475–485.

36. Gething, M. J., R. W. Doms, …, J. White. 1986. Studies on the mechanism of membrane fusion: site-specific mutagenesis of the hemagglutinin of influenza virus. *J. Cell Biol.* 102:11–23.

37. Qiao, H., R. T. Armstrong, …, J. M. White. 1999. A specific point mutant at position 1 of the influenza hemagglutinin fusion peptide displays a hemifusion phenotype. *Mol. Biol. Cell.* 10:2759–2769.

38. Han, X., J. H. Bushweller, …, L. K. Tamm. 2001. Membrane structure and fusion-triggering conformational change of the fusion domain from influenza hemagglutinin. *Nat. Struct. Biol.* 8:715–720.

39. Tamm, L. K., A. L. Lai, and Y. Li. 2007. Combined NMR and EPR spectroscopy to determine structures of viral fusion domains in membranes. *BBA-Biomembranes.* 1768:3052–3060.

40. Lai, A. L., and L. K. Tamm. 2010. Shallow boomerang-shaped influenza hemagglutinin G13A mutant structure promotes leaky membrane fusion. *J. Biol. Chem.* 285:37467–37475.

41. Haque, M. E., H. Chakraborty, …, B. R. Lentz. 2011. Hemagglutinin fusion peptide mutants in model membranes: structural properties, membrane physical properties, and PEG-mediated fusion. *Biophys. J.* 101:1095–1104.

42. Schmidt, N., A. Mishra, …, G. C. Wong. 2010. Arginine-rich cell-penetrating peptides. *FEBS Lett.* 584:1806–1813.

43. Keller, S. L., S. M. Gruner, and K. Gawrisch. 1996. Small concentrations of alamethicin induce a cubic phase in bulk phosphatidylethanolamine mixtures. *BBA-Biomembranes.* 1278:241–246.

44. Staudegger, E., E. J. Prenner, …, K. Lohner. 2000. X-ray studies on the interaction of the antimicrobial peptide gramicidin S with microbial lipid extracts: evidence for cubic phase formation. *BBA-Biomembranes.* 1468:213–230.

45. Prenner, E. J., R. N. A. H. Lewis, …, R. N. McElhaney. 1997. Nonlamellar phases induced by the interaction of gramicidin S with lipid bilayers. A possible relationship to membrane-disrupting activity. *Biochemistry.* 36:7906–7916.

46. Hickel, A., S. Danner-Pongratz, …, G. Pabst. 2008. Influence of antimicrobial peptides on the formation of nonlamellar lipid mesophases. *BBA-Biomembranes.* 1778:2325–2333.

47. Zweytick, D., S. Tumer, …, K. Lohner. 2008. Membrane curvature stress and antibacterial activity of lactoferricin derivatives. *Biochem. Biophys. Res. Commun.* 369:395–400.

48. Tristram-Nagle, S., R. Chan, …, J. F. Nagle. 2010. HIV fusion peptide penetrates, disorders, and softens T-cell membrane mimics. *J. Mol. Biol.* 402:139–153.

49. Tristram-Nagle, S., and J. F. Nagle. 2007. HIV-1 fusion peptide decreases bending energy and promotes curved fusion intermediates. *Biophys. J.* 93:2048–2055.